SEMARAK ILMU PUBLISHING

CFD Letters

Journal homepage:
https://semarakilmu.com.my/journals/index.php/CFD_Letters/index
ISSN: 2180-1363

Numerical Investigation of Flow and Dispersion over Two-Dimensional Semi-Open Street Canyon

Muhammad Fatih Ibrahim[1], Mohd Faizal Mohamad[1,*], Naoki Ikegaya[2], Azli Abd Razak[1]

[1] School of Mechanical Engineering, College of Engineering, Universiti Teknologi MARA, 40450 Shah Alam, Malaysia
[2] Faculty of Engineering Sciences, Kyushu University, 6-1 Kasuga-koen, Kasuga-shi, Fukuoka 816-8580, Japan

ARTICLE INFO

Article history:
Received 11 August 2022
Received in revised form 7 September 2022
Accepted 12 October 2022
Available online 1 February 2023

Keywords:
Semi-open canyon; scalar dispersion; eave; CFD; RANS

ABSTRACT

A semi-open street canyon is able to protect pedestrians from unpleasant situations such as direct sunlight and rain. However, the protruding elements of the two opposite building facades that form the semi-open configuration can affect the air quality of the urban canopy layer (UCL). Therefore, this paper investigated the influence of the eave structures on the flow and pollutant dispersion over an idealized 2D street canyon with a unity aspect ratio. The length of the eaves was varied into 0.25*H* and 0.5*H* (*H* is the building height) and placed either on the leeward wall, the windward wall, or on both building facades located at the same elevation as the street canyon. Numerical simulations were performed using the steady-state Reynolds-averaged Navier-Stokes (RANS) equations in conjunction with Re-Normalization Group (RNG) *k-ε* as the turbulence closure model. The pollutant was released from a line source in the center of the bottom of the target canyon with uniform flow rate. Six different eave configurations were simulated in the wind direction perpendicular to the canyon axis, representing the worst condition of canyon ventilation. The evolution of the primary vortex, which occupied the entire canyon with the characteristic of skimming flow, showed less dependence on the length and position of the eave, except for the longest eave on the windward wall. However, the position of the vortex center depicted opposite results. The pollutant concentration is always higher near the leeward wall, but for the eave that protrudes from the windward wall with a length of 0.5*H*, the pollutant accumulates near the windward region. The ratio of pollutant concentration showed higher concentration in the semi-open configurations compared to the fully open layout as a result of limited penetration of shear flow into the canyon, which leads to deterioration of pollutant removal.

1. Introduction

Wind flow and scalar dispersion in urban areas have attracted the interest of many researchers in recent decades due to the accumulation of pollutants in the street canyon, which negatively affects pedestrian's health. Most studies have been conducted on idealized street canyons rather than real configurations to investigate the mechanism of flow and its interactions with buildings [1-4]. Several parameters have been studied, such as aspect ratio, roof shape, obstacles in the street canyon, and

* *Corresponding author.*
E-mail address: faizal3744@uitm.edu.my (Mohd Faizal Mohamad)

https://doi.org/10.37934/cfdl.15.2.5370

wind direction, but for two-dimensional (2D) street canyons, aspect ratio is the most important parameter to define the flow regime and pollutant dispersion. Aspect ratio can be defined as the ratio of street width to building height and plays an important role in the development of three well-known flow regimes over idealized parallel urban arrays, known as skimming flow, wake-interference flow, and isolated roughness flow [5].

Flow and dispersion over an idealized street canyon under various aspect ratios was first demonstrated by Meroney *et al.,* [1] using wind tunnel experiments. To further elucidate the dispersion phenomena, the behaviour of concentration fluctuations and the interaction between turbulence scales are studied by applying statistical analysis at a unity aspect ratio [6]. Pollutant concentrations are found to be higher on the leeward side than on the windward side because scalars are driven to the leeward side by primary recirculation as part of the skimming flow. The studies are extended to different building shapes, i.e., 2D street canyons, prisms, and cube-shaped buildings, using the numerical approach of RANS equations [7]. In addition, Cheng and Liu [8] and Yazid *et al.,* [9] conducted a series of numerical studies using large-eddy simulations (LES) on the skimming flow regime. All of these studies were conducted on flat roof configuration.

In addition to the flat roof, the effects of different roof shapes are studied experimentally and numerically. Wind tunnel studies have shown that a pitched roof improves ventilation in the canyon area by developing a strong shear above the roof with high turbulence intensity [10]. Numerical studies of different slope angles in different flow regimes have further illustrated the dependence of street canyon flow structure and air quality on roof shape [4,11]. In addition, street canyon vortex dynamics and pollutant distribution are strongly determined by wedge-shaped roof configurations (height and position of the roof peak) [12]. Modification of roofs (shape and pitch) has shown a significant impact on the determination of flow fields and the efficiency of pollutant removal from the street canyon [13]. An extended study conducted with a round roof has shown that turbulent velocities in the street canyon and shear layer depth increase, whereas balconies on the building facades lead to an opposite result [14].

Although a large number of intensive studies have been conducted, most of them have focused on a fully open street canopy configuration, i.e., no obstructions/architectural features at building height that restrict the flow exchange between the street canyon and the flow aloft. In a semi-open design, elevated structures such as eaves, awnings, overhangs, balconies, arcades and platforms are constructed on the building facades [15]. Balconies significantly modify the flow structure in the canyon by reducing mass transfer between the shear and canopy layers and thus increasing pollutant concentrations in pedestrian areas [14,16]. Furthermore, the dimensions of the arcades (height and width) play an important role in the ventilation of the canyon, therefore, careful attention must be paid to avoid negative impacts when designing the arcades [17]. In addition, the results of wind tunnel experiments and large eddy simulation (LES) have shown that protruding overhangs significantly reduced the velocity and turbulence intensity of the street canyon despite their small volume compared to the volume of the buildings [18,19].

Eave is one of the semi-open settings often found in townhouse developments that extend beyond both building facades [20]. It serves to protect pedestrians from direct sunlight, provide parking, and offer a gathering place underneath. However, the design can vary depending on the climatic conditions at a particular site. Several studies have been conducted on semi-open canyon configurations, including a market building, a naturally ventilated shopping center, and enclosed (or semi-open) markets, in which the ventilation performance of the street canyon was investigated [21-23]. Increasing the roof level eave width has resulted to the increment of the in-canyon pollutant concentration due to limited opening for ventilation [24]. However, these studies were carried out

with three-dimensional (3D) building layouts where the ambient flow can enter and exit the canyon through the top and side openings.

There are still too few studies investigating the effects of a semi-open roof on flow and pollutant dispersion in a 2D street canyon where the pollutant can only be purged out through the canyon opening at roof level. Therefore, this study aims to investigate the mechanisms of pollutant dispersion from the urban canopy with different designs of eaves protruding from the building facade and forming a semi-open street canyon. Steady RANS simulations were carried out as they are still the most applicable compared to LES, which require expensive calculations and complex boundary conditions, and are widely used in engineering applications in urban research. To achieve the objectives of this study, two goals are pursued: 1) to investigate the influence of different eave designs on the modification of flow fields within the street canyon, and 2) to evaluate the pollutant distribution within the street canyon under different semi-open roof configurations. This article is organized as follows: The methodology, consisting of the computational domain, building configurations, and numerical setup, is presented in Section 2. In Section 3, the validation results and main findings of the current study are presented. Finally, conclusions are drawn in Section 4.

2. Methodology

2.1 Computational Domain and Building Configurations

The computational domain consists of three identical two-dimensional (2D) street canyon as shown in Figure 1(a). The domain dimensions are $6H \times 4H \times 6H$ for streamwise, spanwise and vertical direction respectively, where H is the building height (H = 0.12 m). All buildings are constructed with a homogeneous height with a constant aspect ratio (ratio between street width, S to building height, H) S/H = 1. The flow is imposed perpendicular to the canyon. In addition, pollutant is released through a continuous ground-level line source located at the middle of the target canyon. Furthermore, Figure 1(b) shows the measurement positions of x/H = -0.25, 0.0 and 0.25 which are constructed for the purpose of validation with experimental data.

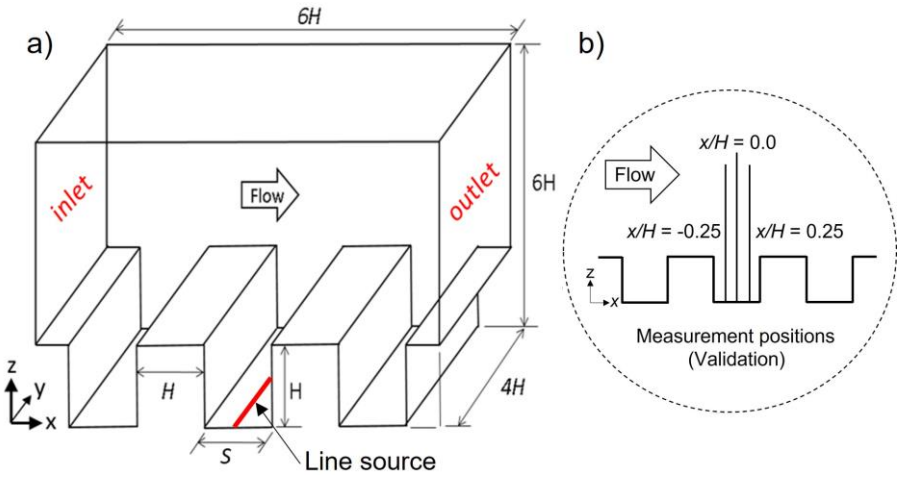

Fig. 1. Schematic diagram of (a) computational domain (b) measurement positions

To ensure the accuracy of the simulated results, a series of grid sensitivity analyses are performed to determine the adequate grid resolution. The domain is discretized into hexahedral elements as shown in Figure 2 that presents the mesh arrangements around the target canyon of no eave (NO) configuration. For this purpose, three meshing sizes, namely coarse (*H*/10), medium (*H*/20) and fine (*H*/40), are generated using structured cells. Grid convergence is estimated through the application of grid convergence index (*GCI*) that is further discussed in sub-section 3.1 [25].

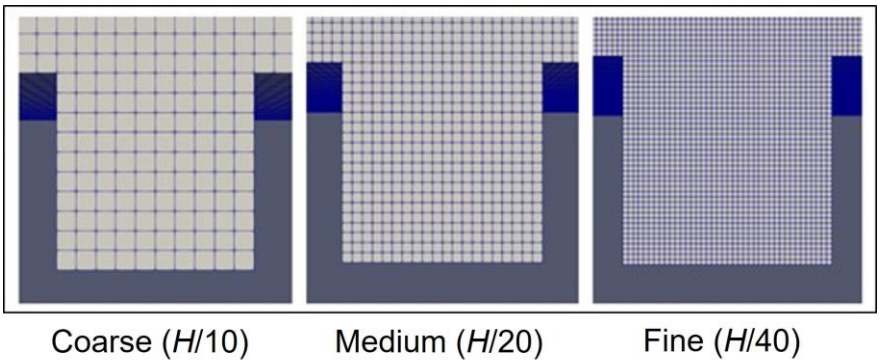

Fig. 2. Mesh resolution adopted for grid sensitivity analysis. *Left*; coarse (*H*/10), *middle*; medium (*H*/20) and *right*; fine (*H*/40)

Figure 3 shows the eave configurations used in the simulations, where the thickness of the eave is kept at 0.1*H*. All simulated cases are designed according to the length and position of the eave. Two different lengths of 0.25*H* and 0.5*H* are considered, while the position is defined by leeward (L), windward (W), or a combination of both. For example, if the length of the eave is 0.25H and is located on the leeward wall, this is referred to as 0.25HL (see Figure 3(b)).

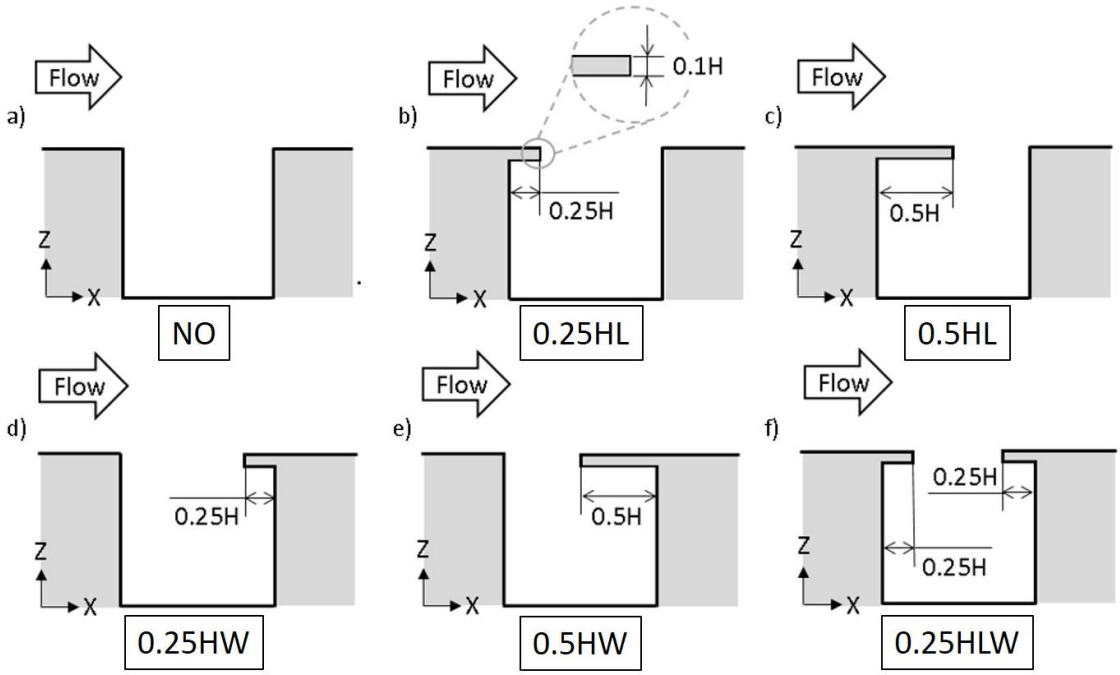

Fig. 3. Configuration of the eave designs (a) no eave (NO) (b) 0.25*H*, leeward (0.25*HL*) (c) 0.5*H*, leeward (0.5*HL*) (d) 0.25*H*, windward (0.25*HW*) (e) 0.5*H*, windward (0.5*HW*) (f) 0.25*H*, leeward windward (0.25*HLW*)

2.2 Governing Equations and Turbulence Model

The simulations are performed by solving the incompressible continuity (Eq. (1)) and RANS equations (Eq. (2)) in combination with passive scalar transport equation. In addition, RNG is used for the turbulence closure model [26]. Several studies conducted on urban configurations have recommended that RNG performs better compared to other $k-\varepsilon$ closure models [27,28].

$$\frac{\partial \bar{u}_i}{\partial x_i} = 0 \tag{1}$$

$$\frac{\partial \bar{u}_i \bar{u}_j}{\partial x_j} = -\frac{1}{\rho}\frac{\partial \bar{p}}{\partial x_i} + \frac{\partial}{\partial x_j}\left[\nu \frac{\partial \bar{u}_i}{\partial x_j} - \overline{u_i' u_j'}\right] \tag{2}$$

where overbar denotes the mean, $\bar{u}_i$ is the mean velocity, ρ is the air density, $\bar{p}$ represents the mean pressure and ν is the fluid kinematic viscosity. Furthermore, *i, j* = 1, 2 and 3 indicate the streamwise, spanwise and vertical directions, respectively. The Reynolds stresses are represented by $-\overline{u_i' u_j'}$ and can be described as Eq. (3).

$$-\overline{u_i' u_j'} = \nu_t \left(\frac{\partial \bar{u}_i}{\partial x_j} + \frac{\partial \bar{u}_j}{\partial x_i}\right) - \frac{2}{3}\delta_{ij} k \tag{3}$$

Here, ν_t represents the kinematic eddy viscosity, δ_{ij} is the Kronecker delta and k denotes turbulent kinetic energy. Transport equation for the pollutant dispersion is governed by the convection-diffusion equation as shown in Eq. (4):

$$\bar{u}_i \frac{\partial \bar{C}}{\partial x_i} = \frac{\partial}{\partial x_i}\left((D + D_t)\frac{\partial \bar{C}}{\partial x_i}\right) + S \tag{4}$$

where $\bar{C}$ represents the mean concentration, D and D_t are the molecular diffusivity and turbulent mass diffusivity $(= \nu_t / Sc_t)$, respectively. Sc_t is the turbulent Schmidt number and S is the pollutant source term.

2.3 Boundary Conditions and Numerical Settings

The periodic boundary conditions are applied on both the streamwise and spanwise boundaries which yield infinitely repeated street canyon. The bottom of the domain and buildings wall are treated as no-slip walls while symmetry boundary conditions are imposed on the top domain. The flow is driven by a momentum source included in the RANS equations to achieve u_{mean} of 8.0 (m/s). Here, u_{mean} is defined as average flow speed over a cross section of the domain. The Reynolds number is based on the freestream velocity and the building height, *H,* of 5.76 x 10^5 which is greater enough than 1.5 x 10^3 to be independent of the Reynolds number [29].

Pollutant is released with a uniform flow rate Q (m^3/s) from continuous ground-level line source. All bottom and building surfaces are impermeable to scalar transport. The periodic boundary conditions for scalar transport are only applied to the spanwise direction and not on the streamwise direction. Scalar can leave the domain via other domain boundaries but cannot enter via them because cyclic boundary conditions are not applied to the advected scalar.

The numerical simulation is performed using the open-source OpenFOAM software. The flow is assumed to be steady state, incompressible and isothermal. The governing equations are solved numerically using the Semi-Implicit Method for Pressure-Linked Equations (SIMPLE) algorithm [30]. Second-order linear interpolation is applied for the gradient terms while second-order discretization schemes are used for both the convection and viscous terms of the governing equations. The convergence is monitored by setting the minimum values of the residuals for pressure to 10^{-5} and 10^{-6} for all remaining equations.

3. Result

3.1 Grid Sensitivity Analysis

Figure 4 shows the normalised velocity profiles for three different grids, namely coarse, medium, and fine, measured at *x/H* = -0.25, 0.0, and 0.25 of the target canyon. The streamwise velocity is represented by *u*, vertical velocity is depicted by *w* and the reference velocity measured at the top of the domain i.e., the freestream velocity, is defined by $u_{fstream}$. In addition to the qualitative comparison, a quantitative evaluation of grid convergence index *(GCI)* is performed to estimate the error in the solution of the medium grid compared to the fine grid. *GCI* is calculated based on Eq. (5) as follow:

$$GCI_{medium} = F_s \left| \frac{r^p[(u_{medium} - u_{fine})/u_{ref}]}{1 - r^p} \right| \tag{5}$$

where $r = 2$ is the linear grid refinement factor, $p = 2$ (formal order of accuracy) due to the second-order discretization schemes used in the simulations and F_s is assigned to 1.25 for the safety factor since three or more grids are considered in the grid sensitivity analysis [31]. The reference velocity u_{ref} is equal to the $u_{fstream}$ in this study.

For streamwise velocity (see Figure 4(a) to Figure 4(c)), a significant difference is observed for the near wall velocity profiles, where the course grid underestimates the reverse flow at all locations compared to the medium and fine grids. In addition, a small discrepancy is observed in the building height where the shear flow dominates. With increasing height (*z/H* > 1.2), no differences are observed between all grid sizes. The calculated *GCI* for three vertical lines is shown in Figure 4(d) to Figure 4(f). In addition, comparison of the different grid sizes for vertical velocity is shown in Figure 5(a) to Figure 5(c) while GCI results are presented in Figure 5(d) to Figure 5(f). Basically, within the street canyon, prediction value by the coarse grid is smaller compared to other grids resolution as seen at the position *x/H* = -0.25 and 0.0 (Figure 5(a) and Figure 5(b)). However, at *x/H* = 0.25 where the shear flow entrains into the canyon, coarse grid shows strong downward flow than medium and fine grids. There are almost no observable differences between those three grids over the building height. Furthermore, the average values of *GCI* for both velocity components for all the lines are less than 1%.

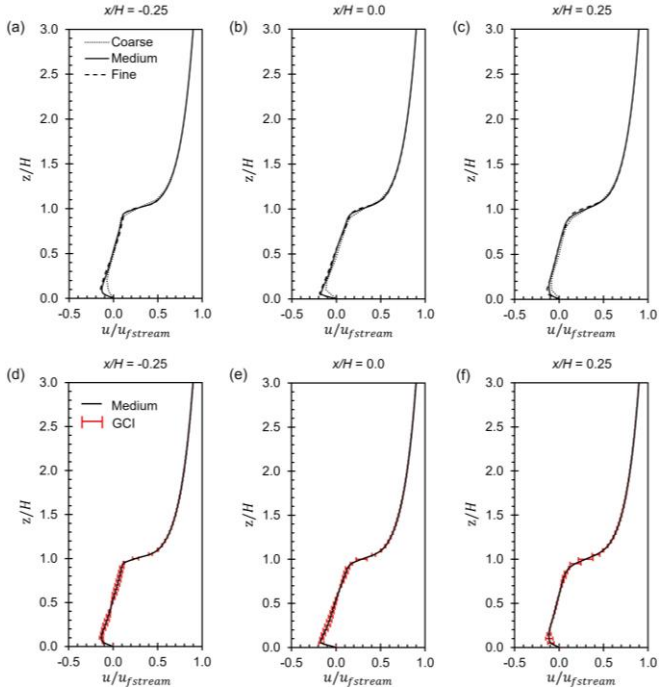

Fig. 4. Grid sensitivity analysis: (a-c) Dimensionless streamwise velocity ($u/u_{fstream}$) comparison on the three different grids, coarse (*H*/10): *dotted line*, medium (*H*/20): *solid line* and fine (*H*/40): *dashed line*. Grid convergence index (*GCI*) along same three vertical lines. (a,d) *x/H* = -0.25; (b,e) *x/H* = 0.0; (c,f) *x/H* = 0.25

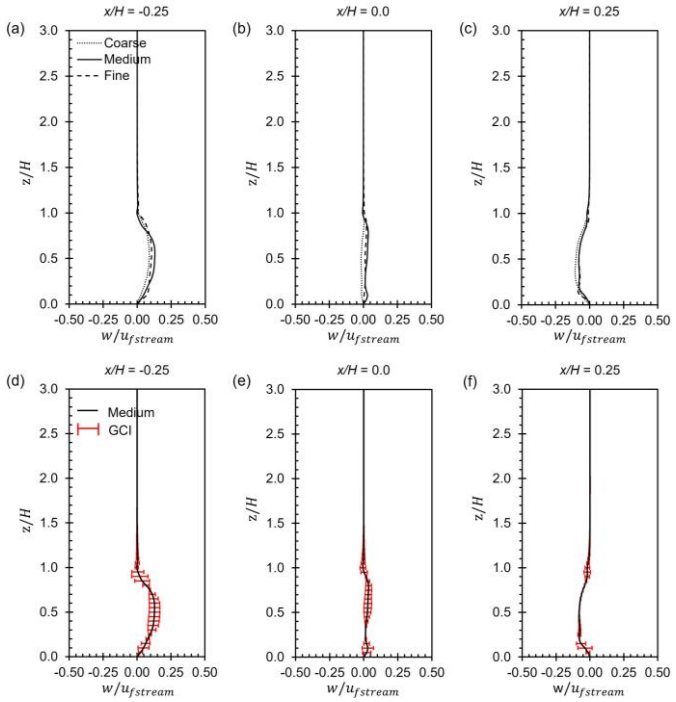

Fig. 5. Grid sensitivity analysis: (a-c) Dimensionless vertical velocity ($w/u_{fstream}$) comparison on the three different grids, coarse (*H*/10): *dotted line*, medium (*H*/20): *solid line* and fine (*H*/40): *dashed line*. Grid convergence index (*GCI*) along same three vertical lines. (a,d) *x/H* = -0.25; (b,e) *x/H* = 0.0; (c,f) *x/H* = 0.25

The results for turbulent kinetic energy (*TKE*) are shown in Figure 6. Figure 6 shows the vertical distribution of the dimensionless turbulent kinetic energy (*TKE*) at *x/H* = -0.25, 0.0 and 0.25 for different grid resolutions. It can be seen that the turbulent kinetic energy profiles are more sensitive to the grid resolution compared to the corresponding velocity profiles (see Figure 4 and Figure 5), especially in the leeward region (*x/H* = -0.25).

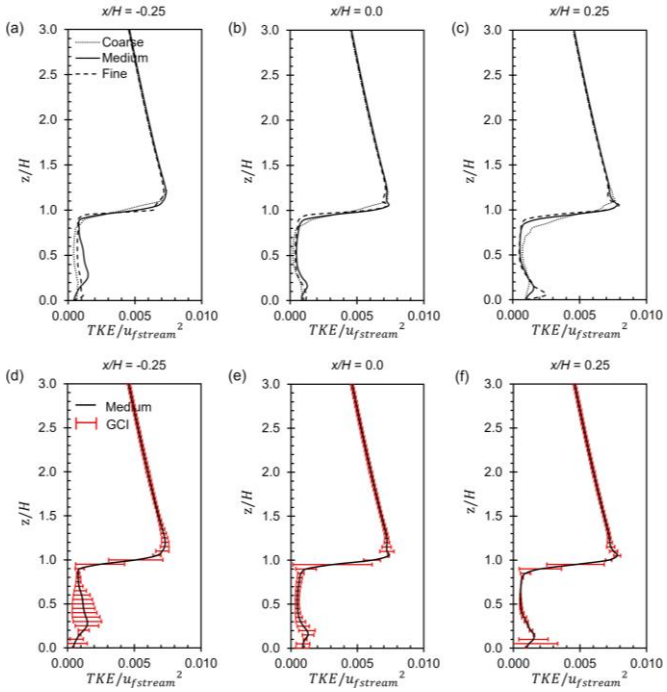

Fig. 6. Grid sensitivity analysis: (a-c) Dimensionless turbulent kinetic energy profiles ($TKE/u_{fstream}^2$) comparison on the three different grids, coarse (*H*/10): *dotted line*, medium (*H*/20): *solid line* and fine (*H*/40): *dashed line*. Grid convergence index (*GCI*) along same three vertical lines. (a,d) *x/H* = -0.25; (b,e) *x/H* = 0.0; (c,f) *x/H* = 0.25

Therefore, it can be concluded that the medium grid provides nearly grid independent. Considering this result and the fact that the difference between the medium and fine grid sizes is very small even though the medium grid requires less computational time, the medium grid size is used for the remainder of the simulations.

3.2 Validation

Validation is an essential process to ensure the credibility of the simulated results. In this study, the first validation is performed for the velocity profiles and the second one is for pollutant concentration. Velocity profiles of the street canyon are compared with the wind tunnel results of Michioka *et al.,* [32] and Brown *et al.,* [33] while pollutant is validated with the results of Meroney *et al.,* [1] and Pavageau and Schatzmann [6]. The validation is conducted for the configuration with no eave (NO) using medium grid size that is already selected through grid sensitivity analysis. Figure 7 shows the vertical distributions of the non-dimensional streamwise and vertical velocities from simulation (solid line) and experimental results (opened circle (EXP_1) and opened square (EXP_2)) measured at *x/H* = -0.25, 0.0 and 0.25. Both velocities are normalized by the velocity at height of 2*H*

(u_{2H}) which is the same as the height measured in the wind tunnel. As shown in Figure 7, the current simulations are in good agreement with experimental results [32,33]. However, a lower vertical velocity is observed at all measured locations compared with wind tunnel experiment of Brown *et al.,* [33] (refer Figure 7(d) to Figure 7(f)). This finding is consistent with the previous LES results and it is suggested that further analysis of the correlation between domain size, grid resolution and recirculation flow speed is required as bigger domain size and finer grid are unable to improve the discrepancies [34].

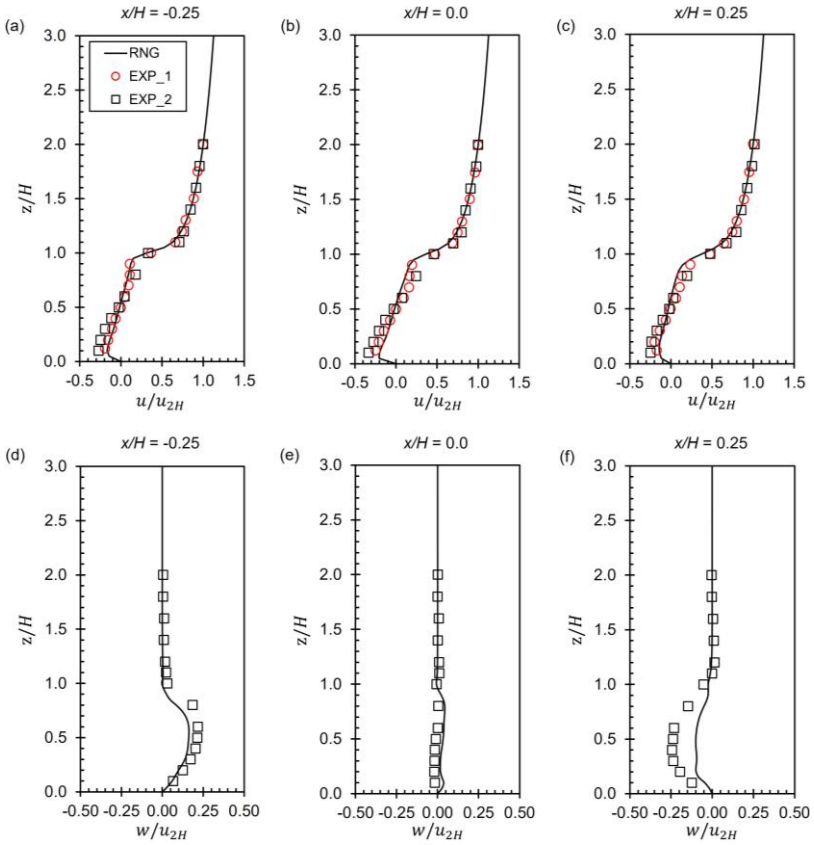

Fig. 7. Comparison of vertical distribution of the streamwise u/u_{2H} and vertical w/u_{2H} velocities between simulation and wind tunnel results at (a)(d) *x/H* = -0.25, (b)(e) *x/H* = 0.0 and (c)(f) *x/H* = 0.25. Wind tunnel experiments; EXP_1 by Michioka *et al.,* [32]: *opened circle*, EXP_2 by Brown *et al.,* [33]: *opened square* and current simulation (RNG): *solid line*

Figure 8 shows the vertical distribution of the dimensionless pollutant concentration along leeward wall (*x/H* = -0.5) and windward wall (*x/H* = 0.5) (refer schematic at top right of Figure 8(b) for the measurement positions) for different turbulent Schmidt numbers, Sc_t. Several studies have shown that Sc_t values are widely distributed from the range of 0.2 to 1.3 [35-39]. Since the value of Sc_t varies according to the case configuration, in this study, several numbers of Sc_t are investigated in order to obtain appropriate value under current simulation conditions. The dimensionless concentration is calculated as,

$$K = \frac{\bar{C}u_{fstream}HP}{Q} \tag{6}$$

where *P* is the length of the line source. Although several Sc_t numbers are tested, only results that correspond to the selected Sc_t values are shown. Finding shows that increasing the Sc_t values resulted to higher concentration prediction of both leeward and windward walls. Despite some discrepancies between numerical result and experimental data, the value Sc_t ranging from 0.3 to 0.4 is seen to be acceptable. Therefore, Sc_t of 0.4 is used for the remaining cases of this study. Even though the value of Sc_t used in this study is smaller compared to several studies, increasing the Sc_t value leads to an overestimation of the concentration because turbulent scalar diffusivity becomes smaller as RNG underestimates the eddy viscosity due to the absence of time-dependent fluctuation within the canyon [36,40,41].

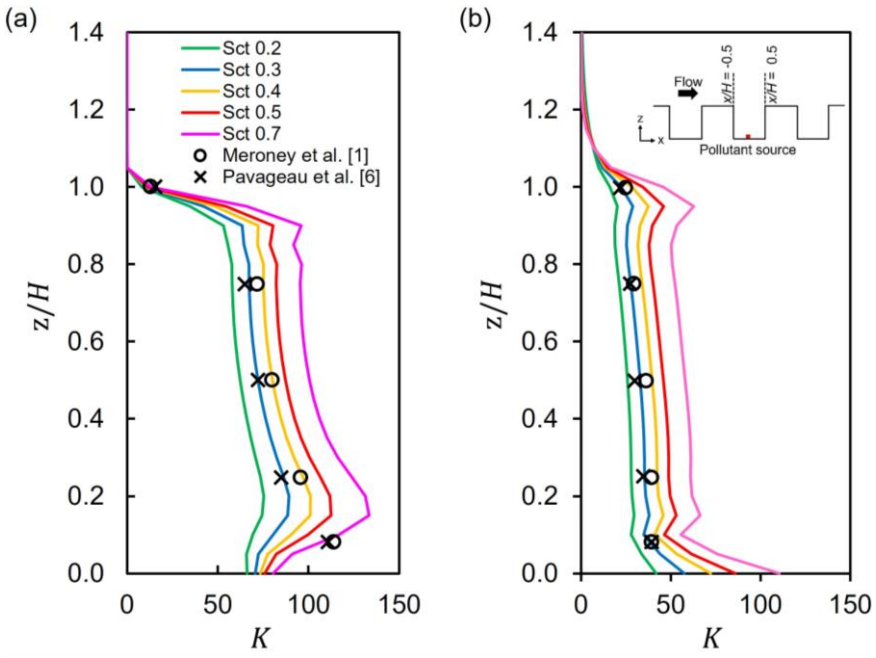

Fig. 8. Vertical distributions of the dimensionless pollutant concentration along (a) leeward wall (b) windward wall with comparison of different turbulent Schmidt Number, *Sct*. (See legends and schematic for the lines classifications and measurement positions, respectively)

3.3 Velocity Contours and Streamlines

Figure 9 shows the velocity streamlines superimposed on the normalized streamwise velocity ($u/u_{fstream}$) contour in *x*-*z* plane for all simulated cases. The result for the NO (Figure 9(a)) shows a well-known skimming flow with a clockwise rotating vortex generated at the centre of the canyon for the cases of perpendicular wind flow direction [5,33,42]. For the building with eave length of 0.25H positioned on the leeward façade (0.25HL) as shown in Figure 9(b), it is observed that the vortex center slightly moves downward as compared to NO. Meanwhile, for 0.5HL (Figure 9(c)), the vortex is horizontally compressed towards the windward wall as the flow is strengthened downward by the downwind building through limited area of opening at the building height. For 0.25HW i.e., eave length 0.25H that is positioned on the windward wall (Figure 9(d)), it is clearly shown that two counter rotating vortices are developed inside the canyon. The position of the vortex center of the clockwise primary vortex is almost identical to the NO while relatively small secondary vortex is observed just underneath the eave of the downwind building. By increasing the eave length on the same position (0.5HW) as depicted in Figure 9(e), the in-canyon flow structure is significantly modified with no primary vortex being developed but only a small clockwise rotating vortex is observed at the top left

corner of the canyon opening. For the eaves that protrudes from both building facades (0.25HLW) as shown in Figure 9(f), the flow structure is almost similar to the 0.25HW but the vortex center is compressed towards the canyon floor.

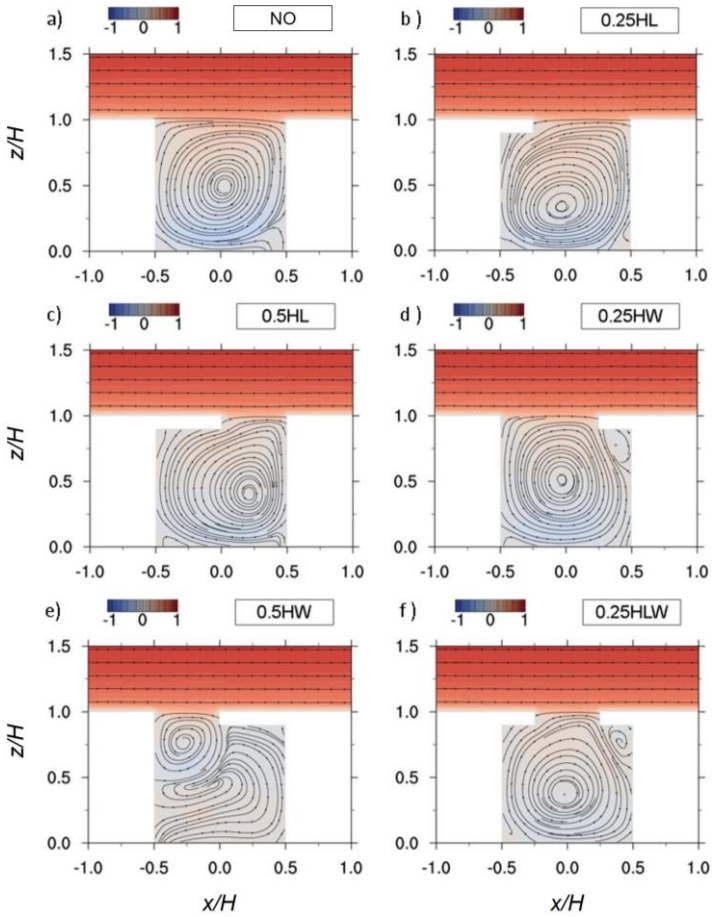

Fig. 9. Normalized velocity contours (a) no eave (NO) (b) 0.25*H*, leeward (0.25*HL*) (c) 0.5*H*, leeward (0.5*HL*) (d) 0.25*H*, windward (0.25*HW*) (e) 0.5*H*, windward (0.5*HW*) (f) 0.25*H*, leeward windward (0.25*HLW*). Colour bar indicates the normalized streamwise velocity

3.4 Turbulent Kinetic Energy (TKE)

The distribution of normalized turbulent kinetic energy, $TKE/u_{fstream}{}^2$ for all configurations is shown in Figure 10. The configuration of NO (Figure 10(a)) shows a high intensity of *TKE* at the corner of the downwind building as the shear layer impinges onto the windward wall. A significant portion of the *TKE* is driven into the canyon while the rest is transported with the boundary layer flow. For the 0.25HL and 0.5HL configurations (see Figure 10(b) and Figure 10(c)), the detachment point has shifted downstream of the eaves length in both cases, resulting in limited flow impingement on the windward wall. Therefore, a reduction in *TKE* production is observed. For the eave that is positioned on the windward wall as shown in Figure 10(d) and Figure 10(e) (0.25HW and 0.5HW), the impingement position has moved upstream which leads to the production of TKE that depicts different in-canyon distribution compared to the eave that protrudes from the leeward façade. In the 0.25HLW configuration (Figure 10(f)), the bulk of the *TKE* does not entrain the canyon as the momentum exchange between the canyon and aloft flow is limited by the eaves.

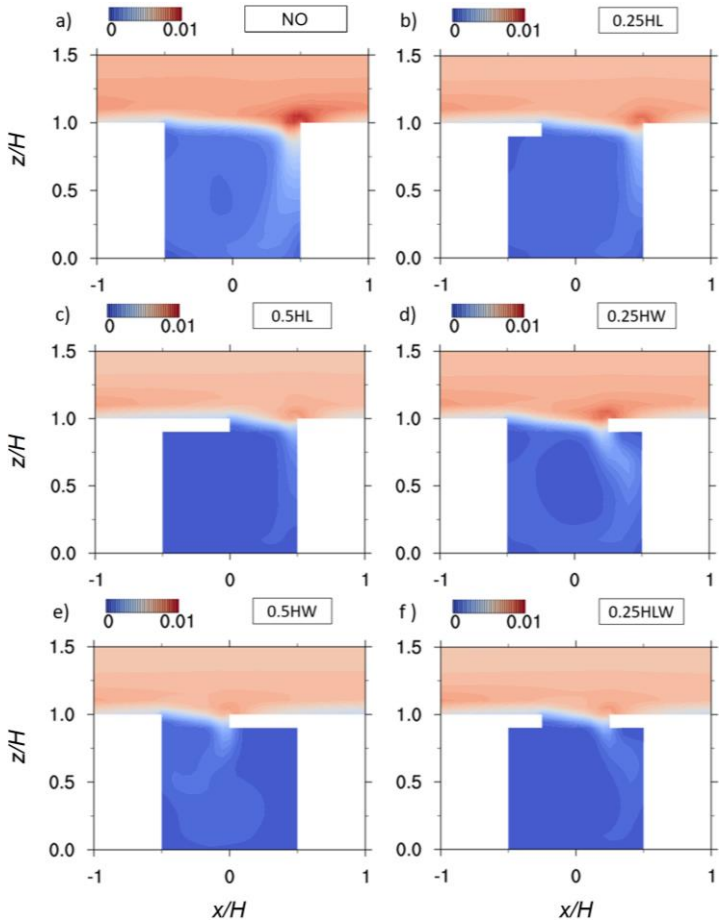

Fig. 10. Normalized turbulent kinetic energy, $TKE/{u_{fstream}}^2$ contours (a) no eave (NO) (b) 0.25*H*, leeward (0.25*HL*) (c) 0.5*H*, leeward (0.5*HL*) (d) 0.25*H*, windward (0.25*HW*) (e) 0.5*H*, windward (0.5*HW*) (f) 0.25*H*, leeward windward (0.25*HLW*). Colour bar indicates normalized turbulent kinetic energy

3.5 Spatial Pollutant Distribution

Figure 11 shows the spatial distribution of the dimensionless pollutant concentration *K* for different eave. For NO, 0.25HL and 0.5HL, the pollutant concentration is always higher on the leeward wall than on the windward wall in which 0.5HL shows a significant higher concentration compared to the former. This is because longer eave length tends to hinder the scalar escaping from the canyon as the upward flow has been restricted. Positioning a different eave length on the windward wall has resulted to different scalar distribution of 0.25HW and 0.5HW as shown in Figure 11(d) and Figure 11(e). Shorter eave on the windward wall shows nearly identical distribution with the building without eave (NO). In contrast, for longer eave (0.5HW), scalars tend to accumulate near the windward wall as they are directed to the region underneath the eave by the streamwise direction flow at the $z/H < 0.5$ region. In addition, the clockwise vortex developed at the top left corner further limits the scalar removal from the canyon. Apart from the eave that protrudes from only one side of the building façade, 0.25HLW shows an almost identical in-canyon scalar distribution with 0.25HL but with higher concentration near the leeward wall as small canyon opening is restricting the fresh air that enters the street canyon.

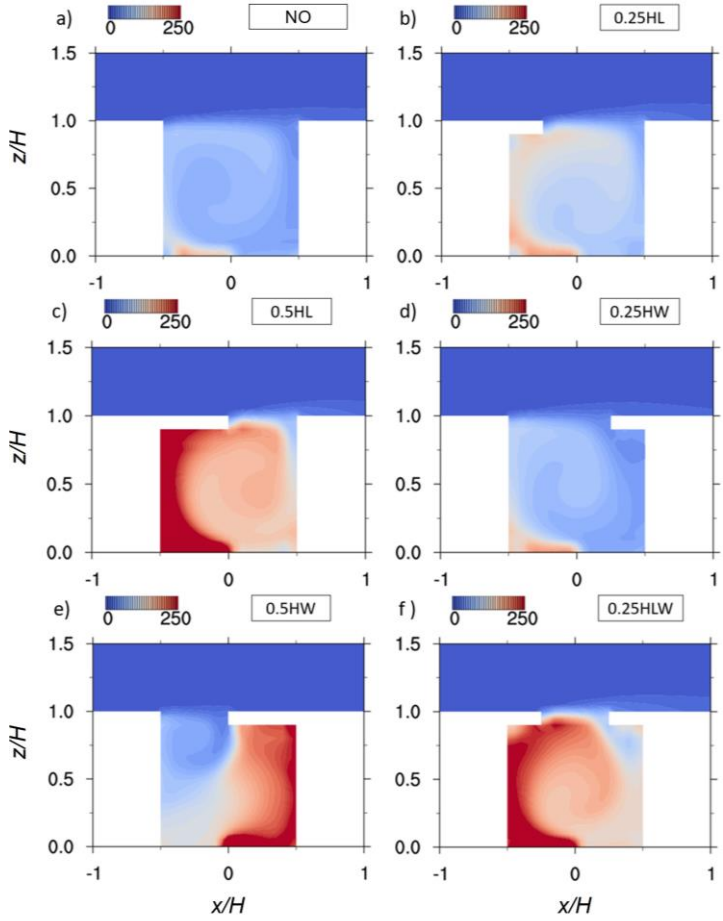

Fig. 11. Normalized pollutant concentration (a) no eave (NO) (b) 0.25*H*, leeward (0.25*HL*) (c) 0.5*H*, leeward (0.5*HL*) (d) 0.25*H*, windward (0.25*HW*) (e) 0.5*H*, windward (0.5*HW*) (f) 0.25*H*, leeward windward (0.25*HLW*). Colour bar indicates the normalized pollutant concentration

3.6 Distribution of Pollutant Concentration on the Wall

Figure 12 shows the dimensionless pollutant concentration along the leeward and windward wall for all cases. On the leeward wall (see Figure 12(a)), NO, 0.25HW and 0.5HW share almost the same concentration along the building height except for the region $z/H < 0.2$. Short eave on the leeward wall (0.25HL) increases the accumulation of the scalar compared to the aforementioned three cases. The highest concentration is recorded by 0.5HL, followed by 0.25HLW. For the windward wall position (Figure 12(b)), the highest concentration profile is given by the longer eave that protrudes from the windward wall (0.5HW), while NO and 0.25HW depict the lowest concentration profile. From the above findings, it can be concluded that the clockwise rotating vortex drives the pollutant to the leeward wall and protruding eave further limits the scalar removal; thus, higher accumulation under the eave is observed. However, for the 0.5HW, the in-canyon flow structure is completely different with other configurations that force the pollutant to accumulate near the windward wall.

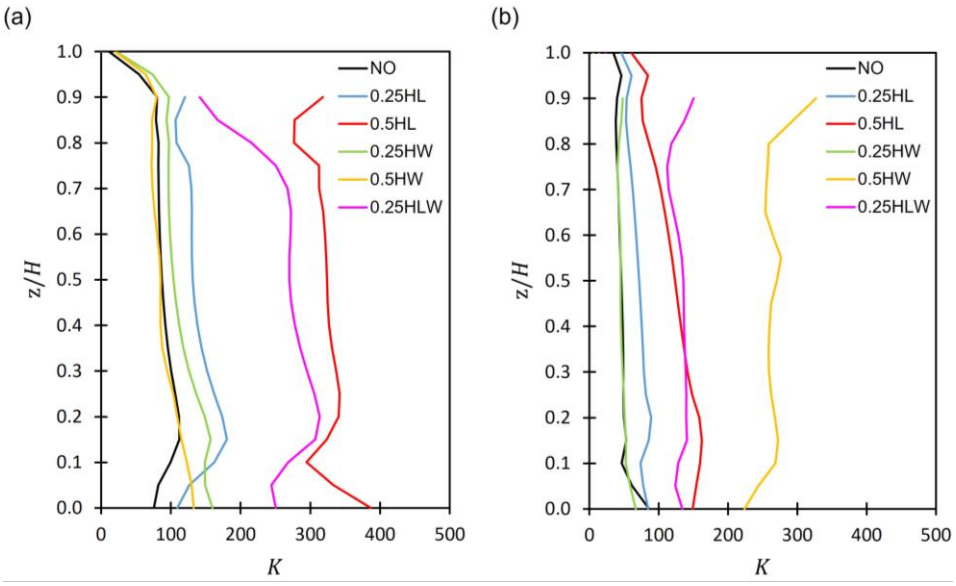

Fig. 12. Vertical distribution of the pollutant concentration along a) leeward wall b) windward wall for all cases

3.7 Pollutant Concentration Ratio, CR

To provide a more detailed analysis on the effect of various eave configurations of the pollutant dispersion within the target canyon, pollutant concentration ratio, *CR*, is calculated as follows,

$$Concentration\ ratio, CR = \frac{<\bar{C}>_{case}}{<\bar{C}>_{ref}} \tag{7}$$

< > indicates the spatial average, *case* refers to the simulated eave configurations, and *ref* is the reference case, i.e., the NO configuration. Figure 13 shows the concentration ratio for all eave configurations, taking NO as the reference case (*CR* =1). 0.5HL and 0.25HW show only a small increase with 1.3 and 1.1, respectively. A further increase in the eave length on each façade i.e., either leeward or windward (0.5HL and 0.5HW), results in a higher concentration ratio, with 0.5HW representing the highest ratio of 3.1. This result is consistent with previous results (see Figure 9(e) and Figure 11(e)) in which flow at the building height prevents the pollutants from escaping the canyon, while they are accumulated in the windward wall region. For the case with eaves protruding from both facades (0.25HLW), the ratio is almost comparable to that of 0.5HL. From these results, it can be concluded that a protruding eave on the building facade increases the accumulation of pollutants in the canyon due to the restricted air exchange between the canopy and the initial layer.

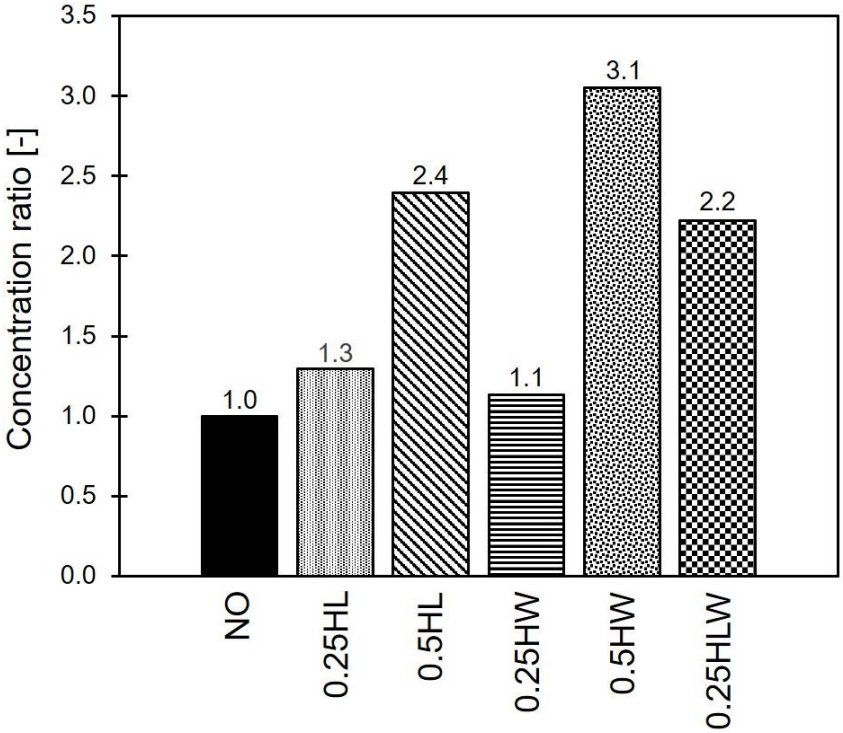

Fig. 13. Effect of eave configurations on the pollutant concentration within the street canyon

4. Conclusions

A series of simulations on the effects of eave designs on the flow within and above idealized 2D semi-open street canyon are performed by means of RANS model with RNG k – ε as the closure model. The eave is positioned either on the windward, leeward or both facades with two different lengths of 0.25H and 0.5H. Pollutant is released through a line source located at the middle of the target canyon floor with constant volumetric flow rate. Several conclusions can be summarized as follows:

a) For NO, 0.25HL and 0.5HL, single vortex is formed within the canyon regardless the length of eave. However, positioning an eave on the windward wall with different length has resulted to different in-canyon flow structure. Furthermore, eaves that protrude from both facades exhibit two counter-rotating vortices. Generally, the location of the vortex center is determined by the position and length of the eave.
b) For the investigated eave configurations under unity aspect ratio, scalar concentration is always higher near the leeward wall regardless its position and length except for the 0.5HL that shows contradict results.
c) Spatial average of scalar concentration of the eave protruding from windward (0.5HW) and leeward (0.5HL) has demonstrated higher pollutant accumulation compared to other eave configurations.

Although the configuration used in this study is still idealized, this finding is expected to provide a view on the complexity of the flow and dispersion in real urban environments. Thus, careful consideration is required to avoid any adverse effect due to the accumulated pollutant within the canyon.

Acknowledgment

This research is funded by a grant from Universiti Teknologi MARA (600-IRMI/MYRA 5/3/LESTARI (0083/2016)).

References

[1] Meroney, Robert N., Michel Pavageau, Stilianos Rafailidis, and Michael Schatzmann. "Study of line source characteristics for 2-D physical modelling of pollutant dispersion in street canyons." *Journal of Wind Engineering and Industrial Aerodynamics* 62, no. 1 (1996): 37-56. https://doi.org/10.1016/S0167-6105(96)00057-8

[2] Baik, Jong-Jin, and Jae-Jin Kim. "A numerical study of flow and pollutant dispersion characteristics in urban street canyons." *Journal of Applied Meteorology* 38, no. 11 (1999): 1576-1589. https://doi.org/10.1175/1520-0450(1999)038<1576:ANSOFA>2.0.CO;2

[3] Takano, Y., and P. Moonen. "On the influence of roof shape on flow and dispersion in an urban street canyon." *Journal of Wind Engineering and Industrial Aerodynamics* 123 (2013): 107-120. https://doi.org/10.1016/j.jweia.2013.10.006

[4] Garau, Michela, Maria Grazia Badas, Simone Ferrari, Alessandro Seoni, and Giorgio Querzoli. "Turbulence and air exchange in a two-dimensional urban street canyon between gable roof buildings." *Boundary-Layer Meteorology* 167, no. 1 (2018): 123-143. https://doi.org/10.1007/s10546-017-0324-4

[5] Oke, Tim R. "Street design and urban canopy layer climate." *Energy and Buildings* 11, no. 1-3 (1988): 103-113. https://doi.org/10.1016/0378-7788(88)90026-6

[6] Pavageau, Michel, and Michael Schatzmann. "Wind tunnel measurements of concentration fluctuations in an urban street canyon." *Atmospheric Environment* 33, no. 24-25 (1999): 3961-3971. https://doi.org/10.1016/S1352-2310(99)00138-7

[7] Meroney, Robert N., Bernd M. Leitl, Stillianos Rafailidis, and Michael Schatzmann. "Wind-tunnel and numerical modeling of flow and dispersion about several building shapes." *Journal of Wind Engineering and Industrial Aerodynamics* 81, no. 1-3 (1999): 333-345. https://doi.org/10.1016/S0167-6105(99)00028-8

[8] Cheng, W. C., and Chun-Ho Liu. "Large-eddy simulation of turbulent transports in urban street canyons in different thermal stabilities." *Journal of Wind Engineering and Industrial Aerodynamics* 99, no. 4 (2011): 434-442. https://doi.org/10.1016/j.jweia.2010.12.009

[9] Yazid, A. W. Muhammad, S. M. Salim, and S. Mansor. "Numerical Simulation of Thermal Atmospheric Conditions in an Idealized Street Canyon: Comparison Between RANS and LES." *Journal of Advanced Research in Fluid Mechanics and Thermal Sciences* 1, no. 1 (2014): 19-27.

[10] Rafailidis, Stylianos. "Influence of building areal density and roof shape on the wind characteristics above a town." *Boundary-Layer Meteorology* 85, no. 2 (1997): 255-271. https://doi.org/10.1023/A:1000426316328

[11] Badas, Maria Grazia, Michela Garau, and Giorgio Querzoli. "How gable roofs change the mechanisms of turbulent vertical momentum transfer: A LES study on two-dimensional urban canyons." *Journal of Wind Engineering and Industrial Aerodynamics* 209 (2021): 104432. https://doi.org/10.1016/j.jweia.2020.104432

[12] Huang, Yuandong, Xiaonan Hu, and Ningbin Zeng. "Impact of wedge-shaped roofs on airflow and pollutant dispersion inside urban street canyons." *Building and Environment* 44, no. 12 (2009): 2335-2347. https://doi.org/10.1016/j.buildenv.2009.03.024

[13] Yassin, Mohamed F. "Impact of height and shape of building roof on air quality in urban street canyons." *Atmospheric Environment* 45, no. 29 (2011): 5220-5229. https://doi.org/10.1016/j.atmosenv.2011.05.060

[14] Llaguno-Munitxa, Maider, Elie Bou-Zeid, and Marcus Hultmark. "The influence of building geometry on street canyon air flow: validation of large eddy simulations against wind tunnel experiments." *Journal of Wind Engineering and Industrial Aerodynamics* 165 (2017): 115-130. https://doi.org/10.1016/j.jweia.2017.03.007

[15] Voordeckers, D., T. Lauriks, S. Denys, P. Billen, T. Tytgat, and M. Van Acker. "Guidelines for passive control of traffic-related air pollution in street canyons: An overview for urban planning." *Landscape and Urban Planning* 207 (2021): 103980. https://doi.org/10.1016/j.landurbplan.2020.103980

[16] Llaguno-Munitxa, Maider, and Elie Bou-Zeid. "Shaping buildings to promote street ventilation: A large-eddy simulation study." *Urban Climate* 26 (2018): 76-94. https://doi.org/10.1016/j.uclim.2018.08.006

[17] Wen, Chih-Yung, Yu-Hsuan Juan, and An-Shik Yang. "Enhancement of city breathability with half open spaces in ideal urban street canyons." *Building and Environment* 112 (2017): 322-336. https://doi.org/10.1016/j.buildenv.2016.11.048

[18] Sato, Tsuyoshi, Aya Hagishima, Naoki Ikegaya, and Jun Tanimoto. "Wind tunnel experiment on turbulent flow field around 2D street canyon with eaves." *Journal of Environmental Engineering (Japan)* 81, no. 723 (2016): 467-476. https://doi.org/10.3130/aije.81.467

[19] Mohamad, Mohd Faizal, Aya Hagishima, Naoki Ikegaya, Jun Tanimoto, and Abd Rahman Omar. "Aerodynamic effect

of overhang on a turbulent flow field within a two-dimensional street canyon." *Engineering Sciences Reports* 37, no. 1 (2015): 1-7.
[20] Nugroho, Agung Murti, Mohd Hamdan Ahmad, and Dilshan Remaz Ossen. "A preliminary study of thermal comfort in Malaysia' s single storey terraced houses." *Journal of Asian Architecture and Building Engineering* 6, no. 1 (2007): 175-182. https://doi.org/10.3130/jaabe.6.175
[21] Kato, Shinsuke, Shuzo Murakami, Takeo Takahashi, and Tomochika Gyobu. "Chained analysis of wind tunnel test and CFD on cross ventilation of large-scale market building." *Journal of Wind Engineering and Industrial Aerodynamics* 67 (1997): 573-587. https://doi.org/10.1016/S0167-6105(97)00101-3
[22] da Graça, Guilherme Carrilho, Nuno R. Martins, and Cristina S. Horta. "Thermal and airflow simulation of a naturally ventilated shopping mall." *Energy and Buildings* 50 (2012): 177-188. https://doi.org/10.1016/j.enbuild.2012.03.037
[23] Kim, Taeyeon, Kwangho Kim, and Byungseon Sean Kim. "A wind tunnel experiment and CFD analysis on airflow performance of enclosed-arcade markets in Korea." *Building and Environment* 45, no. 5 (2010): 1329-1338. https://doi.org/10.1016/j.buildenv.2009.11.016
[24] Hang, Jian, Zhiwen Luo, Mats Sandberg, and Jian Gong. "Natural ventilation assessment in typical open and semi-open urban environments under various wind directions." *Building and Environment* 70 (2013): 318-333. https://doi.org/10.1016/j.buildenv.2013.09.002
[25] Roache, P. J. "Perspective: a method for uniform reporting of grid refinement studies." *Journal of Fluids Engineering* 116, no. 3 (1994): 405-413. https://doi.org/10.1115/1.2910291
[26] Yakhot, V., S. A. Orszag, Siva Thangam, T. B. Gatski, and C. G. Speziale. "Development of turbulence models for shear flows by a double expansion technique." *Physics of Fluids A: Fluid Dynamics* 4, no. 7 (1992): 1510-1520. https://doi.org/10.1063/1.858424
[27] Li, Xian-Xiang, Chun-Ho Liu, and Dennis YC Leung. "Development of ak-ε model for the determination of air exchange rates for street canyons." *Atmospheric Environment* 39, no. 38 (2005): 7285-7296. https://doi.org/10.1016/j.atmosenv.2005.09.007
[28] Sini, Jean-François, Sandrine Anquetin, and Patrice G. Mestayer. "Pollutant dispersion and thermal effects in urban street canyons." *Atmospheric Environment* 30, no. 15 (1996): 2659-2677. https://doi.org/10.1016/1352-2310(95)00321-5
[29] Snyder, William H. *Guideline for fluid modeling of atmospheric diffusion*. Vol. 81, no. 9. Environmental Sciences Research Laboratory, Office of Research and Development, US Environmental Protection Agency, 1981.
[30] Patanker, S. V. "A calculation procedure for heat, mass and momentum transfer in three dimensional parabolic flows." *International Journal of Heat and Mass Transfer* 15 (1972): 1787-1805. https://doi.org/10.1016/0017-9310(72)90054-3
[31] Roache, Patrick J. "Quantification of uncertainty in computational fluid dynamics." *Annual Review of Fluid Mechanics* 29, no. 1 (1997): 123-160. https://doi.org/10.1146/annurev.fluid.29.1.123
[32] Michioka, Takenobu, Ayumu Sato, Hiroshi Takimoto, and Manabu Kanda. "Large-eddy simulation for the mechanism of pollutant removal from a two-dimensional street canyon." *Boundary-Layer Meteorology* 138, no. 2 (2011): 195-213. https://doi.org/10.1007/s10546-010-9556-2
[33] Brown, M., R. Lawson, D. DeCroix, and R. Lee. "Mean flow and turbulence measurements around a 2-d array of buildings in a wind tunnel." In *11th Joint Conference on the Applications of Air Pollution Meteorology*. 2000.
[34] Cheng, W. C., and Chun-Ho Liu. "Large-eddy simulation of flow and pollutant transports in and above two-dimensional idealized street canyons." *Boundary-Layer Meteorology* 139, no. 3 (2011): 411-437. https://doi.org/10.1007/s10546-010-9584-y
[35] Lien, F. S., E. Yee, H. Ji, A. Keats, and K. J. Hsieh. "Progress and challenges in the development of physically-based numerical models for prediction of flow and contaminant dispersion in the urban environment." *International Journal of Computational Fluid Dynamics* 20, no. 5 (2006): 323-337. https://doi.org/10.1080/10618560600898528
[36] Tominaga, Yoshihide, and Ted Stathopoulos. "CFD modeling of pollution dispersion in a street canyon: Comparison between LES and RANS." *Journal of Wind Engineering and Industrial Aerodynamics* 99, no. 4 (2011): 340-348. https://doi.org/10.1016/j.jweia.2010.12.005
[37] Tominaga, Yoshihide, and Ted Stathopoulos. "Turbulent Schmidt numbers for CFD analysis with various types of flowfield." *Atmospheric Environment* 41, no. 37 (2007): 8091-8099. https://doi.org/10.1016/j.atmosenv.2007.06.054
[38] Li, Ye, and T. Stathopoulos. "Numerical evaluation of wind-induced dispersion of pollutants around a building." *Journal of Wind Engineering and Industrial Aerodynamics* 67 (1997): 757-766. https://doi.org/10.1016/S0167-6105(97)00116-5
[39] Baik, Jong-Jin, Jae-Jin Kim, and Harindra J. S. Fernando. "A CFD model for simulating urban flow and dispersion." *Journal of Applied Meteorology* 42, no. 11 (2003): 1636-1648. https://doi.org/10.1175/1520-0450(2003)042<1636:ACMFSU>2.0.CO;2

[40] Liu, Chun-Ho, Mary C. Barth, and Dennis Y. C. Leung. "Large-eddy simulation of flow and pollutant transport in street canyons of different building-height-to-street-width ratios." *Journal of Applied Meteorology* 43, no. 10 (2004): 1410-1424. https://doi.org/10.1175/JAM2143.1

[41] Michioka, Takenobu, and Ayumu Sato. "Effect of incoming turbulent structure on pollutant removal from two-dimensional street canyon." *Boundary-Layer Meteorology* 145, no. 3 (2012): 469-484. https://doi.org/10.1007/s10546-012-9733-6

[42] Ai, Z. T., and Cheuk Ming Mak. "CFD simulation of flow in a long street canyon under a perpendicular wind direction: Evaluation of three computational settings." *Building and Environment* 114 (2017): 293-306. https://doi.org/10.1016/j.buildenv.2016.12.032